Orientation symmetry breakings in shearing liquid crystals

W. H. Han and A. D. Rey
Department of Chemical Engineering, McGill University,
3480 University Street, Montreal, Quebec, Canada H3A 2A7
(Received 1 March 1994)

It has long been an unexplained phenomenon that both out-of-shear-plane [P. Pieranski and E. Guyon, Phys. Rev. Lett. **32**, 924 (1974)] and partially in-shear-plane orientation modes [P. E. Cladis and S. Torza, Phys. Rev. Lett. **35**, 1283 (1975)] of nonaligning nematic liquid crystals between bounding shearing surfaces are experimentally observed. To explain these seemingly mutually exclusive orientation modes, we show that the numerical solutions to the well established Leslie-Ericksen governing equations predict multiple stable steady state orientation patterns, which display the main characteristics of the two experimentally observed orientation modes.

PACS number(s): 64.70.Md, 47.20.Ft, 47.20.Hw, 47.50.+d

This Brief Report is concerned with the flow instabilities, bifurcations, and pattern formation that are present [1–3] in the shear flows of nonaligning rodlike low molar mass nematic liquid crystals. The shear-induced orientation critically depends on the magnitude of reactive parameter λ [4]. When $\lambda \geq 1$, the absence of viscous torques is found when the director aligns uniformly at a positive angle to the flow direction, but when $\lambda < 1$, a steady state nonuniform orientation arises by a balance of elastic and viscous torques. The lack of flow-orienting behavior is captured by the Leslie-Ericksen (LE) nonlinear viscoelastic continuum theory of nematodynamics, in which the velocity $\mathbf{v}$, pressure p, and average molecular orientation unit vector (director) $\mathbf{n}$ are described by the solutions to the coupled force and torque balance equations [4].

Pieranski and Guyon (PG) presented optical measurements, using conoscopy during simple shear flow, of a nonaligning nematic, *p-n*-hexyloxy-benzilidene-*p'*-aminobenzonitrile (HBAB) and found an in-plane (IP) to out-of-plane (OP) orientation transition above some critical shear rate [1]; here IP denotes the orientation state in which $\mathbf{n}$ is restricted to the shear plane defined by the flow direction and the velocity gradient direction, while OP denotes an orientation state having a nonzero component normal to the shear plane. On the other hand, Cladis and Torza (CT) presented qualitatively different experimental results of flow-induced orientation transition for both HBAB and *N-p*-cyanobenzylidene-*p-n*-octyloxyaniline using polarized light microscopy in conjunction with Couette flow [2]. Detailed, but as yet not fully explained, experimentally observed instability phenomena were given in [1,2,5]. The essential difference between the two observations is that at steady state PG detected OP orientation throughout the thickness coordinate, whereas CT detected localized OP orientation at the interface between the center region and boundary region. In addition CT showed in this intermediate shear rate region that OP orientation appears "mysteriously at the interface between the boundary layer and the effective gap [5]," even though the director in the center region remains IP. This hybrid orientation pattern showing both IP and OP orientations is also sketched in [6], based on experimental observations [7]. In addition, recent conoscopic measurements showed hybrid IP and OP orientation during shearing of polymeric nematic(poly-γ-benzyl glutamate) [8]. The need to have a full understanding of these phenomena has been recently emphasized in [3].

It is now well known that the full LE equations for shear flow of nonaligning nematics predict that the IP solutions become unstable to OP perturbations [9] whenever the controlling Ericksen number is larger than a critical value $\mathcal{E}_{co}$; here $\mathcal{E}$ is a characteristic ratio between viscous and elastic torques [$\mathcal{E} = \gamma_1 hU/(\prod_{i=1}^{3} K_{ii})^{\frac{1}{3}}$]; γ_1, h, U, and K_{ii} are the rotational viscosity, gap spacing, moving top plate speed, and Frank curvature elastic moduli, respectively. Recently detailed bifurcation diagrams, containing a wide variety of stationary branches, have been computed for both low molar mass and polymeric nematics [10,11]. Rheological predictions [12] using LE theory are in exellent agreement with experimental measurements [13,14] and suggest that OP orientation during shear flow is the rule rather than the exception.

The main objective of this Brief Report is to present numerical data, obtained from the proven [15] and reliable LE equations, that provide a plausible explanation for the starkly different observations of [1,2]. We integrate the full LE equation for simple shear start-up flows of a well characterized nonaligning nematic 4-*n*-octyl-4'-cyanobiphenyl (8CBP), for which a full set of experimentally measured Leslie viscosity coefficients and Frank elasticity constants [10] are available; here we use values for $T = 35\,^{\circ}\mathrm{C}$. The flow direction is along the x axis and the thickness and vorticity directions are along the y, and z axes, respectively. The plate separation is $h = 3.5 \times 10^{-4}$ m, and the upper plate (H=1) is set, at t=0, in motion with a fixed velocity U with respect to the bottom plate (H=0); here H denotes the dimensionless thickness (y/h). Details of the numerical methods we used are found in [11]. The solution vector consists of the velocity field ($v_x(y,t)$, $v_z(z,t)$) and the director field ($n_x(y,t)$, $n_y(y,t)$ $n_z(y,t)$). The boundary conditons are noslip for the velocities [$v_x(H=1,t)=U$, $v_x(0,t)=v_z(0,t)=v_z(1,t)=0$] and fixed homeotropic director anchoring [$\mathbf{n}$=(0,1,0)] at the bounding surfaces (H=0,1). The *reference initial condition*, referred to as

IC1, consists of no flow $[v_x(H)=v_z(H)=0,\ 0<H<1]$ and a randomly perturbed orientation field $\mathbf{n}_0^*=(n_{0x}^*,\ n_{0y}^*,\ n_{0z}^*)=(\epsilon_x,\ 1+\epsilon_y,\ \epsilon_z)/[\epsilon_x^2+(1+\epsilon_y)^2+\epsilon_z^2]^{\frac{1}{2}}$ $(t=0,0<H<1)$, where the maxium magnitude of the small random perturbation is $||\ \epsilon_i\ ||_{max}=10^{-2}, i=x,y,z$.

To meet the objective of this paper we show the effects of the variation of the Ericksen number and of symmetry reflection transformations of the small initial OP orientation perturbations on the evolutions of the director profiles $(n_x(H,t), n_y(H,t), n_z(H,t))$ for shear start-up flows. The three types of reflection-transformed initial OP orientation perturbations (n_{z0}) with respect to the *reference initial orientation condition* (IC1) are (i) IC2, coordinate reflection about the centerline $H=\frac{1}{2}$, $n_{z0}(H)=n_{z0}^*(1\text{-}H)$; (ii) IC3, OP orientation reflection, $n_{z0}(H)=-n_{z0}^*(H)$; and (iii) IC4, coordinate and OP orientation reflection, $n_{z0}=-n_{z0}^*(1-H)$. It is shown below that at low $\mathcal{E}$ the stable solutions are achiral (A), but at higher $\mathcal{E}$ they are chiral (C). In addition these solutions can have a right or left bias; (R,L) denotes right-twisted and left-twisted bias for achiral, and right-handed and left-handed bias for chiral solutions. Further symmetry breakings, denoted by $(+,-)$, indicate whether the location of n_x minimum is above $(+)$ or below $(-)$ the centerline. The eight stable steady state solutions discussed here are $AR\pm$, $AL\pm$, $CR\pm$, and $CL\pm$ and all are obtained by the virtually identical initial conditions presented above.

We next present the full computed bifurcation diagram that captures all the symmetry breakings explained above in the vicinity of $110<\mathcal{E}<150$. Figure 1(a) shows a three-dimensional bifurcation diagram of $n_{z,center}$ and $n_{x,center}$ as a function of $\mathcal{E}$. The arrows indicate the selected orientation mode among the stable modes at steady state from a given initial condition; if $\mathcal{E}<\mathcal{E}_{PC}=133$ the achiral mode is selected, while if $\mathcal{E}\geq\mathcal{E}_{PC}$ the chiral mode is the stable steady state. It is found that when $\mathcal{E}<\mathcal{E}_{PC}$, the IC1 leads to $AR+$, IC2 to $AR-$, IC3 to $AL+$, and IC4 to $AL-$, and when $\mathcal{E}\geq\mathcal{E}_{PC}$, IC1 leads to $CL+$, IC2 to $CR-$, IC3 to $CR+$, and IC4 to $CL-$. The typical orientation for the two modes (chiral: $\mathcal{E}=133$ and achiral: $\mathcal{E}=130$) can be clearly distinguished using the director's unit sphere [16]. Figures 1(b) and (c) show the steady state director tip trajectories on two unit spheres for $\mathcal{E}=133$ $(CL+)$ and $\mathcal{E}=130$ $(AR+)$, on $0\leq H\leq 1$. The arrows indicate the increasing H direction, the bottom plate $(H=0)$ is denoted by A, and $(H=\frac{1}{4},\frac{1}{2},\frac{3}{4},1)$ by (B,C,D,A). The figure shows that the chiral trajectory has one singular point (A) while the achiral trajectory has two singular points (A and C). The asymmetry is seen by reversing the path on the shown orbits.

To prove that these symmetry breakings are not numerical artifacts, we have performed a systematic parametric study that unequivocally confirms the existence of four asymmetric stable steady state solutions for each orientation mode. Figure 2 shows the parametric connections between the chiral and achiral modes and their eight asymmetric patterns ($AR\pm$, $AL\pm$, $CR\pm$, and $CL\pm$). The director mode and pattern exchanges from a given initial condition (IC1) and $\mathcal{E}$ are established by four

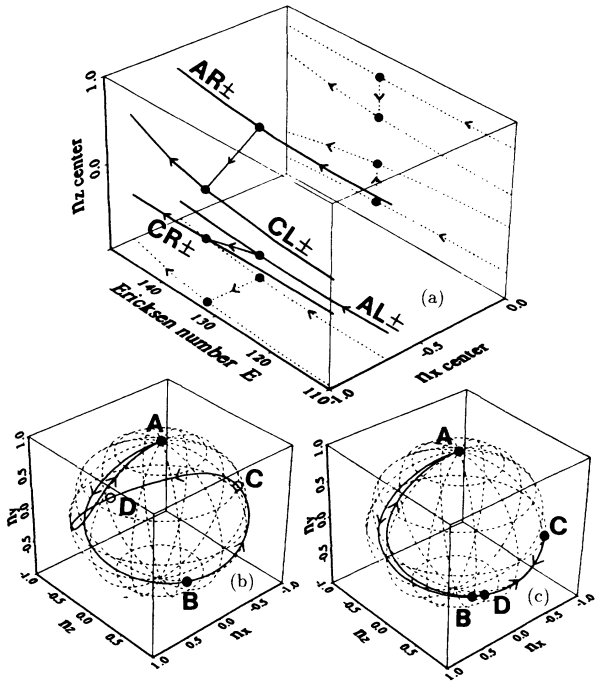

FIG. 1. (a) Three-dimensional steady state bifurcation diagram for shear flow of 8CBP with homeotropic anchoring at a temperature $T=35\,^{\circ}\mathrm{C}$. Arrows indicate the selected steady state for the given $\mathcal{E}$ and initial condition. Dotted lines are orthogonal projections of the three-dimensional solid lines onto the $n_{z,center}=0$, and $n_{x,center}=0$ planes. The discontinous switch between solutions is indicated by an arrowed line segment. (b) and (c) show typical director trajectories on unit spheres, parameterized with the thickness coordinate, for (b) $CL+$ orientation $(\mathcal{E}=133)$ and (c) $AR+$ orientation $(\mathcal{E}=130)$. The arrows indicate the increasing thickness coordinate (H), and $H=(0,\frac{1}{4},\frac{1}{2},\frac{3}{4},1)$ are denoted by the dots (A,B,C,D,A); open and filled dots denote hidden and visible locations, respectively.

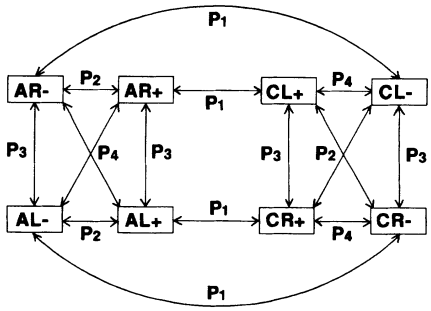

FIG. 2. Path diagram for multiple stable steady state director patterns with respect to the Ericksen number $\mathcal{E}$ and the initial orientation condition. P_i $(i=1,2,3,4)$ identifies the route of pattern exchange. For a given initial orientation $\mathbf{n}_0^*$, P_1 is the variation of $\mathcal{E}$. For a given $\mathcal{E}$, P_2 is for $n_{z0}(H)=n_{z0}^*(1-H)$, P_3 for $n_{z0}(H)=-n_{z0}^*(H)$ and P_4 for $n_{z0}(y)=-n_{z0}^*(1-H)$. See the text for an example.

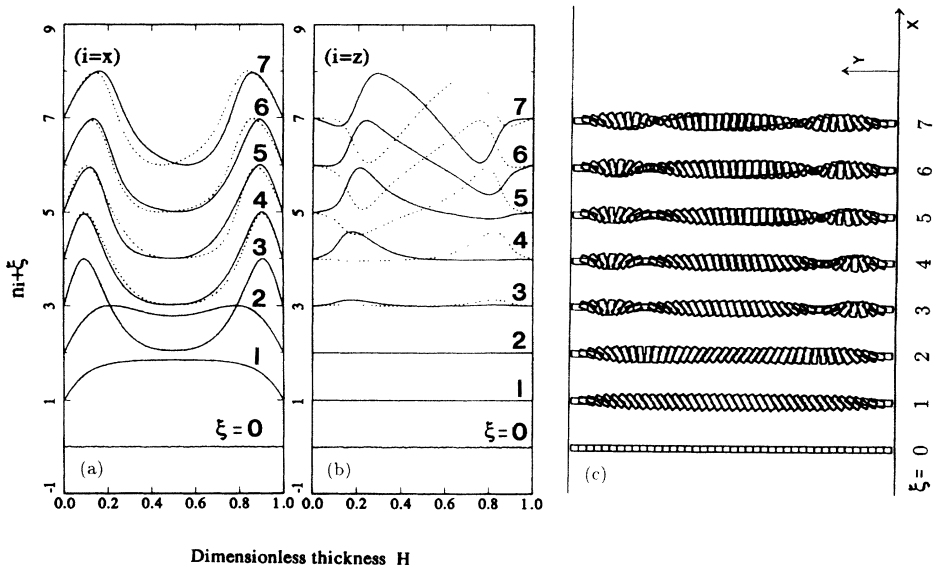

FIG. 3. Three-dimensional director field **n** as a function of time during shear startup flow for $\mathcal{E}$=133. Solid lines correpond to the initial condition [IC1: $n^*_{z0}(H)$, $\xi = 0$] and dotted lines to IC2 [$n^*_{z0}(1-H)$, $\xi = 0$]. Except for the n_z component, IC1 and IC2 are identical. IC1 (IC2) leads to the $CL+$ ($CR-$) solution. The corresponding times (shift factor) are 9.380 ($\xi = 1$), 51.32 ($\xi = 2$), 113.3 ($\xi = 3$), 131.7 ($\xi = 4$), 163.1 ($\xi = 5$), 194.5 ($\xi = 6$), and 317.1 ($\xi = 7$, steady state); time is in seconds. (a) $n_x(H)$ as a function of time, (b) $n_z(H)$ as a function of time $H = \frac{y}{h}$, and (c) corresponding computed three-dimensional orientation visualizations for $CL+$.

routes (P_1, P_2, P_3, and P_4), which are (i) changing $\mathcal{E}$ (P_1), (ii) using IC2 (P_2), (iii) using IC3 (P_3), and (iv) using IC4 (P_4). For example, when one obtains the AR pattern using $\mathcal{E} = 132 < \mathcal{E}_{PC}$ and IC1, the CR pattern can be obtained by taking the P_3 route and then the P_1 route ($\mathcal{E} = 134 > \mathcal{E}_{PC}$). In what follows we show how this solution multiplicity explains the existence of OP and mixed IP-OP modes observed by [1,2].

We next present two ($CL+$ and $CR-$) of the four asymmetric chiral (higher $\mathcal{E}$) solutions. Figure 3(a) shows n_x as a function of time and dimensionless thickness ($H = \frac{y}{h}$) for $\mathcal{E} = 133$ ($U = 5.754 \times 10^{-5}$ $\frac{m}{s}$). Increasing the shift factor ξ represents increasing time; see the figure caption. Solid lines correspond to the reference initial condition IC1 and dotted lines to IC2. The condition IC1 gives rise to the asymmetric steady state profile

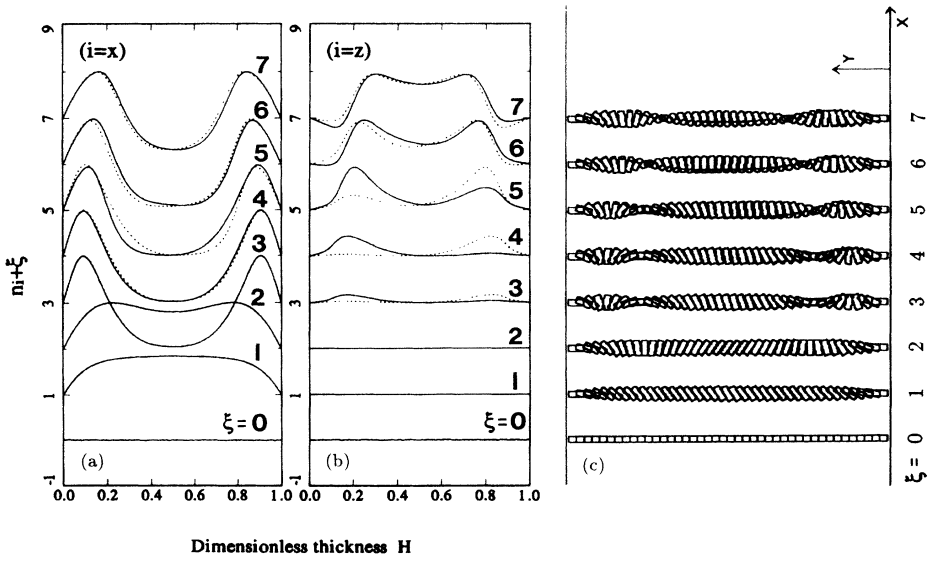

FIG. 4. Three-dimensional director field **n** as a function of time during shear start-up flow for $\mathcal{E}$=130. Solid lines correpond to IC1 and dotted lines to IC2. IC1 (IC2) leads to the $AR+$ ($AR-$) solutions. The corresponding times (shift factor) are 9.380 ($\xi = 1$), 51.59 ($\xi = 2$), 119.2 ($\xi = 3$), 129.7 ($\xi = 4$), 161.2 ($\xi = 5$), 192.6 ($\xi = 6$), and 363.5 ($\xi = 7$, steady state); time is in seconds. (a) $n_x(H)$ as a function of time, (b) $n_z(H)$ as a function of time $H = \frac{y}{h}$, and (c) corresponding computed three-dimensional orientation visualizations for $AR+$.

$CL+$ (ξ=7). When a coordinate-reflected OP initial orientation condition (IC2) is used, a mirror-image asymmetric steady state profile $CR-$ (dotted line, $\xi = 7$) appears at steady state. Figure 3(b) shows the corresponding $n_z(H,t)$ evolution in solid lines for IC1 and in dotted lines for IC2. The appearance of OP orientation follows from a reduction of the elastic energy and a reduction of the shear viscosity. The elastic energy reduction is due to the replacement of high energy splay-bend deformation by low energy twist deformation. The reduction of the shear viscosity follows the ordering of the Miesowicz shear viscosities for rodlike nematics [4]. Line 7 of Fig. 3(b) shows that the fundamental characteristic of these chiral solutions is the presence of two OP orientation peaks of similar amplitude but of different sign. The evolution shown in the figure is a two stage process. The early stage consists of the nucleation and growth of a single OP orientation peak; the location of this peak is explained by differential rotation dynamics [11]. The second pattern formation stage is the growth of the second OP orientation peak in an opposite direction to the already developed first peak; the selection of rotation sense is dictated by the lower elastic energy path. Although the initial first three profiles (ξ=0,1,2) of the two solutions are virtually identical, the small initial difference between IC1 and IC2 eventually leads to opposite orientation screw senses (L, R) and to the opposite asymmetry ($\pm$). Figure 3(c) shows the corresponding three-dimensional visualizations of director profile evolutions for $CL+$, where one can clearly see that the OP orientation *appears at the interface between the bounding surface and center region.* The computations show that at steady state ($\xi = 7$) the center region orientation is virtually IP, which is in very good agreement with CT's experimental observations [2,5].

We next show two ($AR+$ and $AR-$) of the four asymmetric achiral (lower $\mathcal{E}$) solutions. Figure 4(a) shows n_x as a function of time and dimensionless thickness ($H=\frac{y}{h}$) for $\mathcal{E} = 130$ ($U = 5.624 \times 10^{-5}$ $\frac{m}{s}$). The solid line corresponds to IC1 (ξ=0) and shows an asymmetric stable steady state profile $AR+$ (ξ=7). The dotted line corresponds to IC2 and shows a different asymmetric stable steady state orientation pattern $AR-$. The subtle difference between IC1 and IC2 again leads to two asymmetric modes, but with a lesser degree of asymmetry than for $\mathcal{E}$=133. Figure 4(b) shows the corresponding $n_z(H,t)$ evolution for IC1 (solid lines) and IC2 (dotted lines).

For $\mathcal{E}$=130 (achiral) the pattern formation is again a two stage process, as for $\mathcal{E} = 133$. The early stage for both chiral and achiral solutions is similar. The second stage for the achiral solution is characterized by the growth of a second OP orientation peak in the same direction as the first peak; the selection of rotation sense is dictated by the lower elastic energy path. Figure 4(c) shows the corresponding three-dimensional visualization of director profile evolution for $AR+$, where the directors at steady state ($\xi = 7$) are OP and close to the vorticity direction, which is in very good agreement with PG's experimental observation [1].

Summarizing, we give a plausible explanation of the contrasting director structures of the two modes observed experimentally that is based on the actual numerical solutions to the proven nonlinear nonplanar LE equations. In addtion we present a comprehensive characterization consisting of eight asymmetric director patterns and the routes of director pattern exchange that are predicted by the LE equations for shear flow. Small differences in $\mathcal{E}$ and initial condition for a uncomplicated flow history (shear start-up flow) is shown to cause exchanges between two modes and their four asymmetric director patterns. Further study is necessary to assess the importance of the circular streamlines, found in Couette flow [17], on the OP orientation transition phenomena discussed here.

This work is supported by a research grant from Natural Science and Engineering Research Council of Canada.

[1] P. Pieranski and E. Guyon, Phys. Rev. Lett. **32**, 924 (1974).
[2] P. E. Cladis and S. Torza, Phys. Rev. Lett. **35**, 1283 (1975).
[3] L. Lam and J. Prost, *Solitons in Liquid Crystals* (Springer-Verlag, New York, 1992).
[4] P. G. de Gennes, *The Physics of Liquid Crystals* (Clarendon Press, Oxford, 1974).
[5] P. E. Cladis and S. Torza, in *Colloid and Interface Science, Vol. IV, Hydrosols*, edited by M. Kerker (Academic Press, New York, 1976).
[6] P. Manneville, Mol. Cryst. Liq. Cryst. **70**, 223 (1981).
[7] P. Pieranski, these de Doctorat d'Etat, Université Paris-Sud, Orsay, 1976.
[8] M. Srinivasarao, Ph. D. thesis, Carnegie Mellon University, Pittsburgh, 1990.
[9] I. Zuniga and F. M. Leslie, Liq. Cryst. **5**, 725, (1989).
[10] W. H. Han and A. D. Rey, J. Non-Newt. Fluid Mech. **48**, 181 (1993).
[11] W. H. Han and A. D. Rey, Phys. Rev. E **49**, 597 (1994).
[12] W. H. Han and A. D. Rey, J. Rheol. (to be published).
[13] D. Gu, A. M. Jamieson, and S. Wang, J. Rheol. **36**, 985 (1993).
[14] D. Gu and A. Jamieson, Macromolecules **27**, 337 (1994).
[15] F. M. Leslie, in *Advances in Liquid Crystals*, edited by G. H. Brown (Academic, New York, 1979), Vol. 4.
[16] R. N. Thurston and F. J. Almgren, J. Phys. (Paris) **42**, 413 (1981).
[17] I. Zuniga, Phys. Rev. A **41**, 2050 (1990).